Supplementary Information (SI) for Journal of Materials Chemistry A.

Supplementary Information

Self-protecting interlocked electrodes for highly efficient and stable alkaline seawater electrolyzers

Mingming Yin [a, b], Xiongjie Jia [a, b, d], Yukun Sun [a, b], Zhipeng Zhan [a, b], Tianshou Zhao [c, *], Haoran Jiang [a, b, d, *]

[a] Department of Energy and Power Engineering, Tianjin University, Tianjin 300072, China

[b] State Key Laboratory of Engines, Tianjin University, Tianjin 300072, China

[c] Department of Mechanical and Energy Engineering, Southern University of Science and Technology, Shenzhen 518055, China

[d] National Industry-Education Platform of Energy Storage, Tianjin University, Tianjin 300072, China

[*] Corresponding author

E-mail address: zhaots@sustech.edu.cn; jianghaoran@tju.edu.cn

Experimental section

Chemicals

Iron (III) chloride hexahydrate (98%, J&K Scientific), ammonium hydrogen carbonate (AR, Macklin), ruthenium oxide powder (99.9%, Aladdin), platinum on carbon (Pt 20%, Aladdin), potassium hydroxide (85%, Aladdin), nickel nitrate hexahydrate (99.0%, Aladdin), cobalt nitrate hexahydrate (99.0%, Aladdin), ammonium molybdate (99.0%, Macklin), phosphate-buffered saline (PBS) (pH 7.0), and Ni foam (0.5 mm) were used.

Synthesis of amorphous NiFe (oxy)hydroxide on Nickel foam

First, 0.8 mmol $FeCl_3$ powder was added to 60 mL ethanol solution, which was ultrasonicated for around 5 minutes to obtain a homogeneous solution A. A nickel foam (3x3 cm) was immersed in the solution for 12 hours. Subsequently, 4.5 mmol NH_4HCO_3 was added to solution A to obtain solution B. The nickel foam, which has been immersed in solution A, was further immersed in solution B for 6 hours to obtain a Ni/Fe (oxy)hydroxide electrode, named (NiFe)OOH.

Electrodeposition of graphene oxide onto (NiFe)OOH

The obtained (NiFe)OOH was submerged in a graphene oxide aqueous solution (GO 1mg/ml solution in phosphate-buffered saline) for 3 hours, followed by the adoption of an electrodeposition method with an electrodeposition voltage of -0.9 V to -1.5 V and electrodeposition durations of 300 sec, 500 sec and 700 sec. The electrodeposition process occurred within a three-electrode electrochemical cell, where (NiFe)OOH served as the working electrode, Hg/HgO acted as the reference electrode, and a graphite rod was used as the counter electrode. This process allowed for the deposition of a graphene oxide layer onto the (NiFe)OOH electrode, resulting in (NiFe)OOH/graphene oxide electrode, hereafter referred to as (NiFe)OOH GO.

Synthesis of $Ni(Co)MoO_4/MoO_2$ nanorod arrays

$Ni(Co)MoO_4$ cuboids were synthesized onto nickel foam via a hydrothermal process. A 3x3 cm piece of nickel foam was submerged in a 60 mL aqueous solution comprising nickel nitrate (ranging from 0 to 0.04 M), cobalt (ranging from 0 to 0.04 M), and ammonium molybdate (0.01 M), all contained within a Teflon autoclave (named Ni^4, Co^1Ni^3, Co^2Ni^2, Co^3Ni^1 and Co^4 according to the ratio of cobalt to nickel). The autoclave was then heated to 150°C for 6 hours in a drying oven. Subsequent to rinsing with deionized water, the $Ni(Co)MoO_4$ cuboids were successfully formed on the nickel foam. Lastly, the synthesized $Ni(Co)MoO_4$ cuboids underwent heat treatment at 500°C for 2 hours in a H_2/Ar atmosphere (with a composition of 5:95), resulting in the production of the MoO_2 electrocatalyst anchored onto $Ni(Co)MoO_4$ cuboids.

Preparation of Pt/C and RuO_2 electrode on commercial Ni foam

The Pt/C and RuO_2 working electrode was fabricated on Ni foam with the assistance of Nafion solution. 10 mg Pt/C or RuO_2, 50 µL Nafion, 700 µL isopropanol, and 250 µL DI water were mixed and ultrasonicated for 30 min to prepare a homogeneous dispersion. The loading of Pt/C and RuO_2 catalyst on Ni foam is ~ 0.5 and 1.5 mg/cm^2.

Structure characterizations

SEM, as well as corresponding elemental mapping and EDX analysis, were carried out with Apreo S (FEI) and Phenom XL (FEI). Metallographic diagrams were investigated by Axiolab5 (ZEISS). HRTEM was performed using a Tecnai G2 F20 (FEI) scanning TEM. XPS experiments were carried out on a 5000 Versaprobe III (PHI) system using Al Ka radiation. XRD patterns were recorded on a D8 FOCUS (Bruker) using Cu-Ka radiation. UV-vis spectra were recorded with UV-1900i (Shimadzu). Raman spectroscopy measurements were recorded using a Labram HR Evolution (Horiba) system with an excitation wavelength of 532 nm. FTIR was performed using a VERTEX 80v (Bruker). The electrochemical tests were carried out on VSP-300 (Biologic) Potentiostat.

Electrochemical measurements

All electrochemical tests were performed at room temperature. The electrochemical OER and HER were carried out in a three-electrode system. A standard Hg/HgO electrode and a graphite rod were used as the reference and counter electrodes, respectively. The Hg/HgO reference electrode has a potential of 0.098 V vs. standard hydrogen electrode. The potential versus RHE (E_{RHE}) was calculated using the equation $E_{\mathrm{RHE}} = E_{\mathrm{Hg/HgO}} + 0.098\ \mathrm{V} + 0.0592\ \mathrm{V} \times \mathrm{pH}$, where $E_{\mathrm{Hg/HgO}}$ is the potential recorded versus Hg/HgO. OER and HER polarization curve measurements were performed by LSV at a scan rate of 5 mV s^{-1}. Electrochemical impedance spectra (EIS) were measured at an overpotential of 300 mV (OER) and 200 mV (OER) from 0.1 Hz to 100 kHz with an amplitude of 10 mV. The double-layer capacitance (C_{dl}) values were obtained from the CV curves at various scan rates to investigate the electrochemically active surface areas (ECSA). Stability tests were carried out under constant current densities of 500 mA cm^{-2} at room temperature. Alkaline seawater was a natural seawater solution (Bohai Sea, 38°34′N, 118°4′E) of 1.0 M KOH.

Cell assembly

The used membrane electrode assembly (MEA) consists of an anion-exchange membrane (X37-50 Grade T), (NiFe)OOH GO as anode and Ni(Co)MoO_4/MoO_2 as cathode. The cell voltage of alkaline exchange membrane (AEM) electrolyzers was tested on a VSP-300 electrochemical workstation at a scan rate of 5 mV s^{-1}. The flowing 1 M KOH and alkaline seawater were used as an electrolyte and the temperature of the electrolyte can be controlled at 25 °C to 60 °C by a constant temperature heating chamber. The corresponding energy conversion efficiency was calculated according to the following equations:

H_2 production rate @ 1 A cm^{-2}

$= (j\ \mathrm{A\ cm^{-2}})\ (1\ e^{-}/1.602 \times 10^{-19}\ \mathrm{C})\ (1\ \mathrm{H_2}/2\ e^{-})$

$= 1\ \mathrm{A\ cm^{-2}} / (1.602 \times 10^{-19}\ \mathrm{C} \times 2)$

$= 5.18 \times 10^{-6}\ \mathrm{mol\ H_2\ cm^{-2}\ s^{-1}}$

LHV of H_2

$= 120\ \mathrm{kJ\ g^{-1}\ H_2} = 2.42 \times 10^{5}\ \mathrm{J\ mol^{-1}\ H_2}$

H_2 power out

$= (5.18 \times 10^{-6}\ \mathrm{mol\ H_2\ cm^{-2}\ s^{-1}}) \times (2.42 \times 10^{5}\ \mathrm{J\ mol^{-1}}) = 1.254\ \mathrm{W\ cm^{-2}}$

Electrolyzer power (Co^1Ni^3 || (NiFe)OOH GO) @ 1 A cm^{-2}

$= (1\ \mathrm{A\ cm^{-2}})\ (1.79\ \mathrm{V}) = 1.79\ \mathrm{W\ cm^{-2}}$

Efficiency of Co^1Ni^3 || (NiFe)OOH GO

= (H_2 Power out) / (Electrolyzer power)

= 1.254 W cm^{-2} / 1.79 W cm^{-2} = 70.1%

Faradaic efficiency calculations

Derived from the faraday law (1.1) and the ideal gas equation (1.2), we derived a combined equation to calculate the theoretical oxygen evolution flow in V_{O_2} [m^3 s^{-1}] for a 100 % faradaic efficiency.

$$It = nzF$$

* MERGEFORMAT (1.1)

$$pV = nRT$$

* MERGEFORMAT (1.2)

$$V_{O_2} = \frac{IRT}{zFP}$$

* MERGEFORMAT (1.3)

in which I represents the applied current in [A], t is the time in [s], n is the amount of substances in [mol], z = 4 represents the electrons transferred per ion, F = 96485.33 s A mol^{-1} represents the faradaic constant, p = 101400 Pa (determined) is the atmospheric pressure, V is the gas volume in [m^3], R = 8.314 kg m^2 s^{-2} $mol^{-1}K^{-1}$is the ideal gas constant, T = 298.15 K (determined) is the temperature, and V_{O_2} is the gas evolution rate of O_2 in [m^3 s^{-1}].

The obtained flow and the mass flow controlled V_{N_2} flow = 100 ml min^{-1} were used to obtain the theoretical gas concentrations in [%] for a 100 % faradaic efficiency using equation (1.4):

$$c_{gas_{theor.}}[\%] = \left(\frac{V_{O_2}}{V_{O_2} + V_{N_2}} \right) g100$$

* MERGEFORMAT (1.4)

The faradaic efficiency (FE) in [%] was calculated using the theoretical $c_{gas_{theor.}}$ and the nominal $c_{gas_{nor\min al}}$ measured in equation (1.5). The nominal gas concentration is the average value of the last 5 min of the 30 min step.

$$FE[\%]=\left(\frac{c_{gas_{nor\,\min\,al}}}{c_{gas_{theor.}}}\right)g100 \qquad \text{\textbackslash* MERGEFORMAT (1.5)}$$

Density functional theory calculation

Slab models with a vacuum layer of 15 Å are built to simulate the migration of chloride ions and hydroxide ions through the reaction interface. The slab of graphene oxide is based on a monolayer graphite (0 0 0 1) with defects in a 4×4×1 supercell. All DFT calculations were carried out using Vienna *ab-initio* simulation package (VASP)[1] with the Perdew-Burke-Ernzerhof (PBE) generalized gradient approximation (GGA)[2]. Projector-augmented-wave (PAW) potentials[3] were used to take into account the electron-ion interactions. The energy cutoff was set as 500eV for the plane wave-basis expansion and the convergence criteria of the electron self-consistent loop was set to 10^{-7}eV. The geometry of initial states (IS) and final states (FS) was optimized with a conjugate gradient algorithm until the forces acting on the atoms were less than 0.01 eV/Å. The Brillouin zone was sampled on a 1×1×1 Gamma grid. The transition states (TS) were found using the climbing-image nudged elastic band method (CINEB) was adopted[4]. 9 images were interpolated and the convergence criteria of forces was set to 0.03 eV/Å.

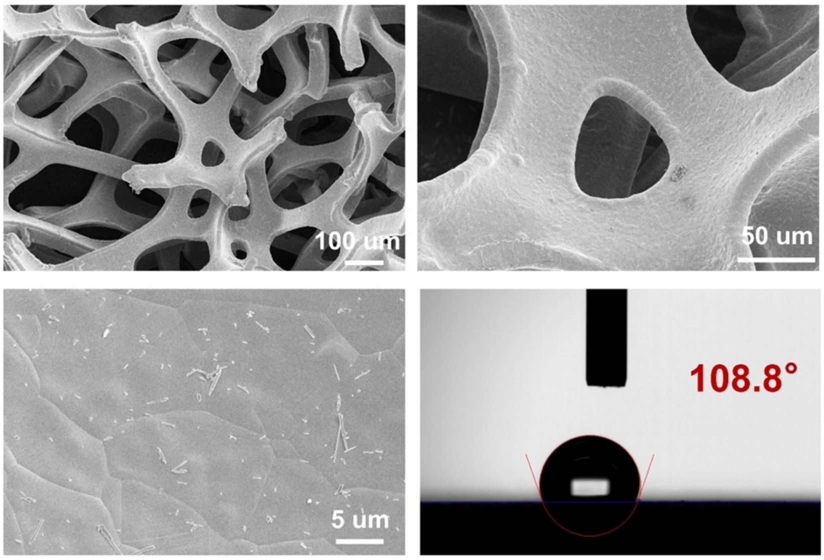

Fig. S1. SEM images and water contact angle of blank nickel foam.

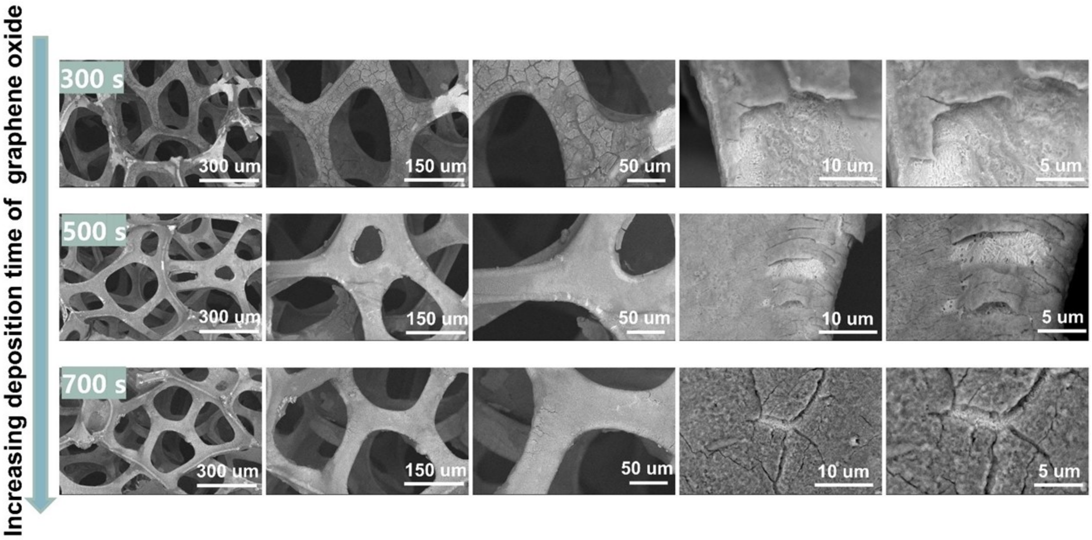

Fig. S2. SEM images of (NiFe)OOH GO with different deposition time.

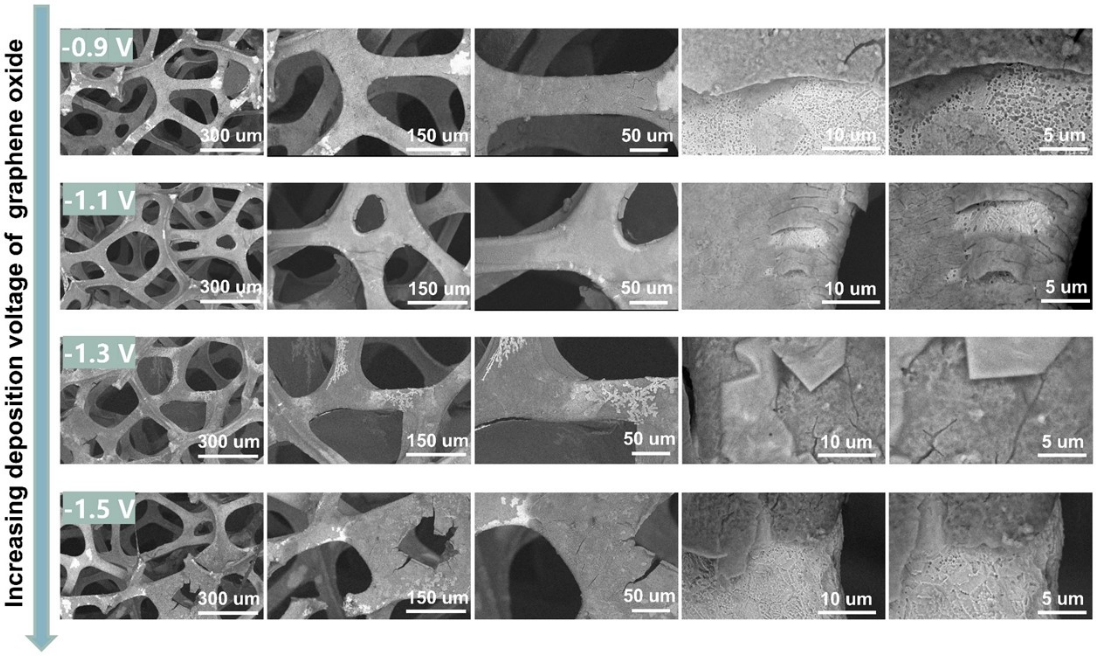

Fig. S3. SEM images of (NiFe)OOH GO with different deposition voltages.

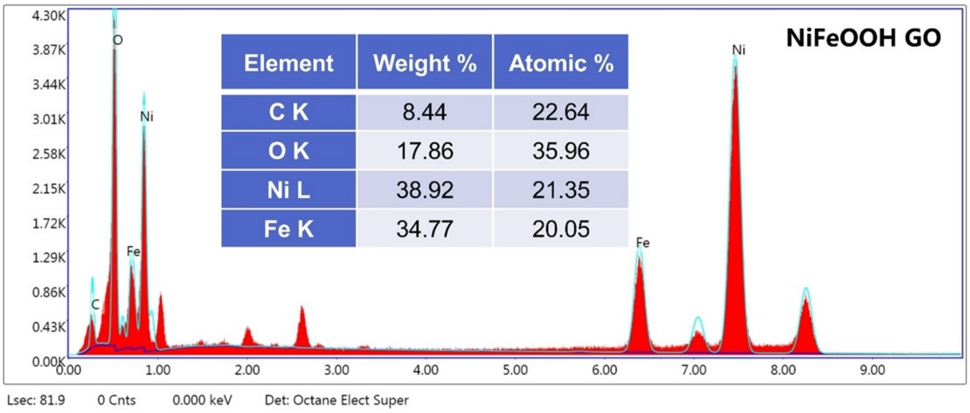

Element	Weight %	Atomic %
C K	8.44	22.64
O K	17.86	35.96
Ni L	38.92	21.35
Fe K	34.77	20.05

Fig. S4. Elemental content result of the (NiFe)OOH GO electrode.

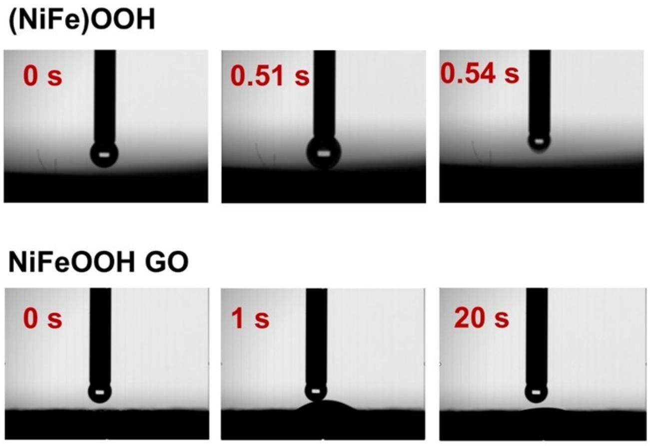

Fig. S5. Water contact angle of (NiFe)OOH and (NiFe)OOH GO.

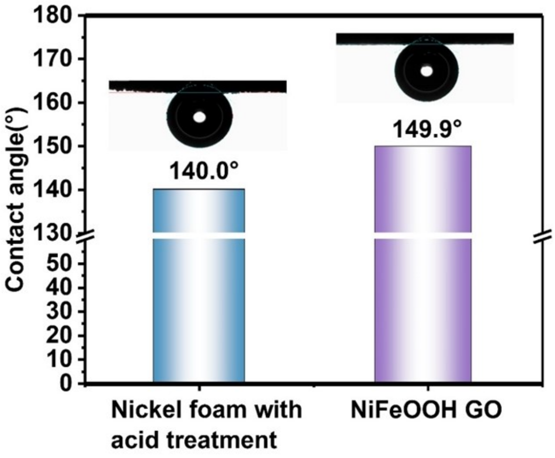

Fig. S6. Air contact angle of nickel foam with acid treatment and (NiFe)OOH GO.

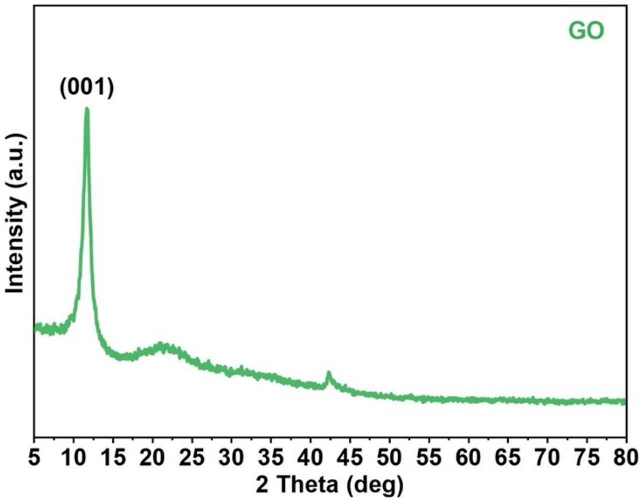

Fig. S7. XRD patterns of GO powder.

Graphene oxide has the unit structure consisting of several oxidized graphene-like sheets. The thickness of the stacking sheets along the c-axis is called the “stack height”. This expression is often used for micrographite unit structures of disordered carbon. The stack height is expressed as L_c. The stack height can be replaced with the average number of stacking layers for showing the stacking structure more clearly. The average number of stacking layers is calculated as follows[5]:

$$\text{Average numbers of stacking layers} = \frac{L_c}{d_{001}} + 1 \tag{1.6}$$

$$L_c = 0.94 \times \frac{0.15418}{\frac{FWHM_{GO}}{180}\pi \times \cos(\frac{2\theta}{360}\pi)} \tag{1.7}$$

The stack height (L_c) is determined through application of the Scherrer equation to the full width at half maximum (FWHM) of the (001) diffraction peak of graphene oxide (GO), in conjunction with the interlayer spacing (d_{001}) derived from Bragg equation. As evidenced by Fig. S7, the FWHM of the GO (001) peak is measured to be 0.74. Through application of Eq. 1.7, the calculated L_c value of 11.23 corresponds to an average stacking layer number of 1.96, confirming the predominantly multilayer nature of the GO structure.

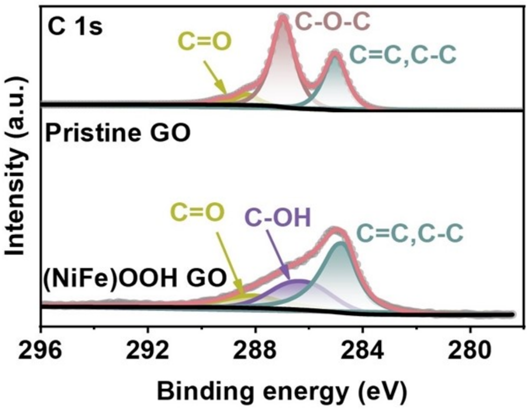

Fig. S8. High-resolution XPS spectra of C 1s for pristine GO and (NiFe)OOH GO electrode.

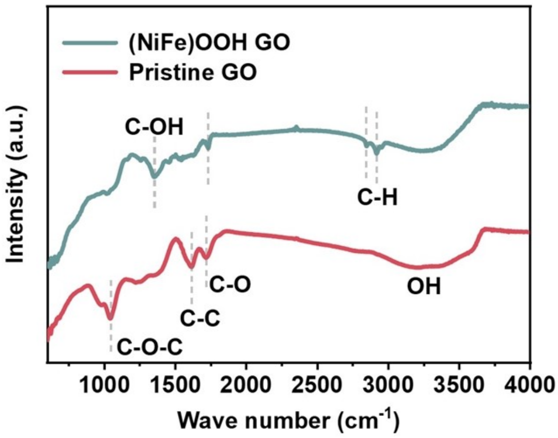

Fig. S9. FTIR spectra for the pristine GO and NiFeOOH GO electrode.

The pristine GO spectrum exhibits characteristic vibrational modes at 1046 cm^{-1} (C-O-C stretching), 1366 cm^{-1} (-OH bending), 1618 cm^{-1} (sp^2-hybridized C=C group), and 1722 cm^{-1} (carboxylic C=O stretching), along with a broad absorption band above 3250 cm^{-1} corresponding to hydroxyl groups and intercalated water molecules[6]. Following electrodeposition, the (NiFe)OOH GO electrode demonstrates a marked attenuation of oxygen-related vibrational modes, indicative of the partial removal of oxygen-containing functional groups. The most pronounced spectral modification involves the significant reduction in C-O stretching vibration intensity, which serves as a characteristic signature of GO reduction[7]. Furthermore, the emergence of new vibrational bands at 2851, 2923, and 1357 cm^{-1} emerged provides compelling evidence for the conversion of sp^2 to sp^3 hybridization in (NiFe)OOH GO structure, concomitant with the formation of C-H and C–OH[8].

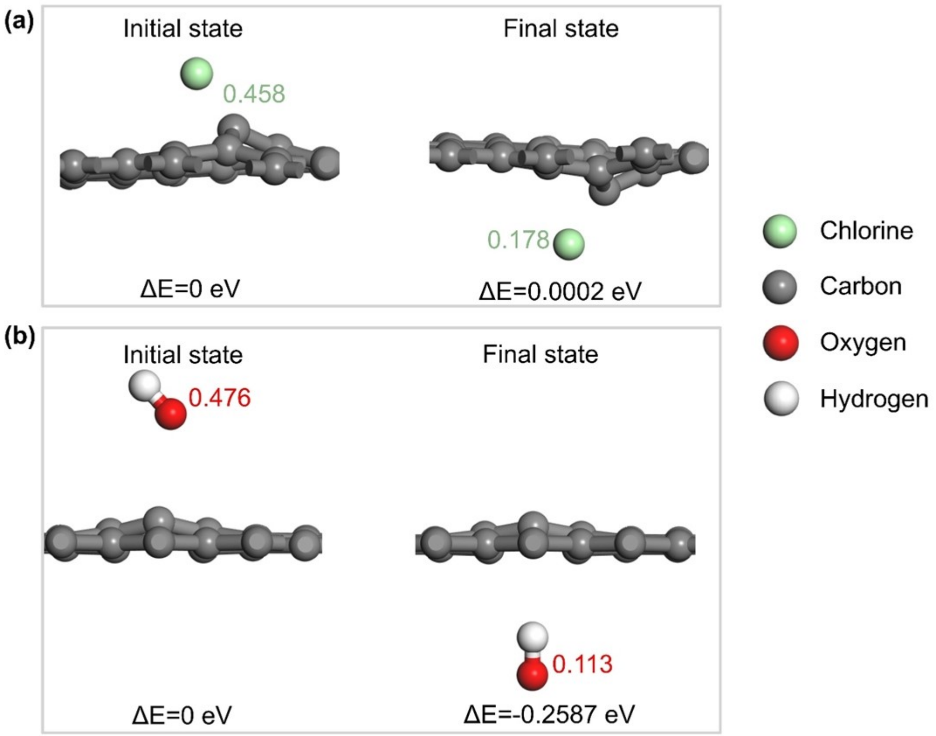

Fig. S10. The initial and final state structures of active substances traversing graphene defect layers. The Initial and final states of the migration process of (a) chloride ions and (b) hydroxide ion. The green numbers in the Fig. represent the absolute coordinates of the chloride ions in the direction perpendicular to the graphene surface, while the red numbers signify the absolute coordinates of the oxygen atoms in the same perpendicular direction. The ΔE denotes the change in energy, with the initial state serving as the reference point.

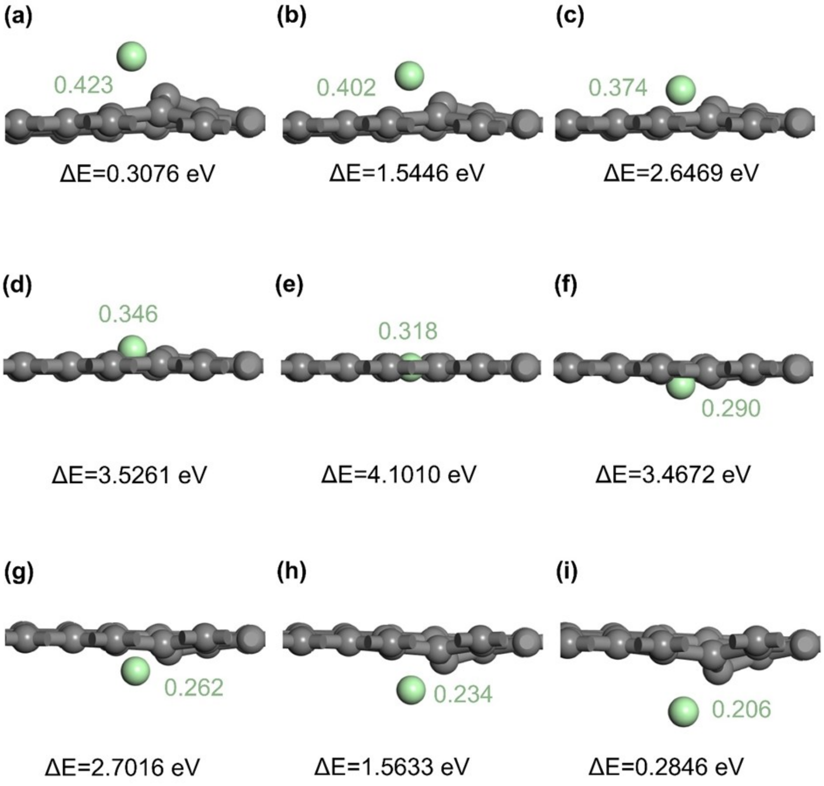

Fig. S11. Molecular structure and energy changes in each state during chloride ion migration.

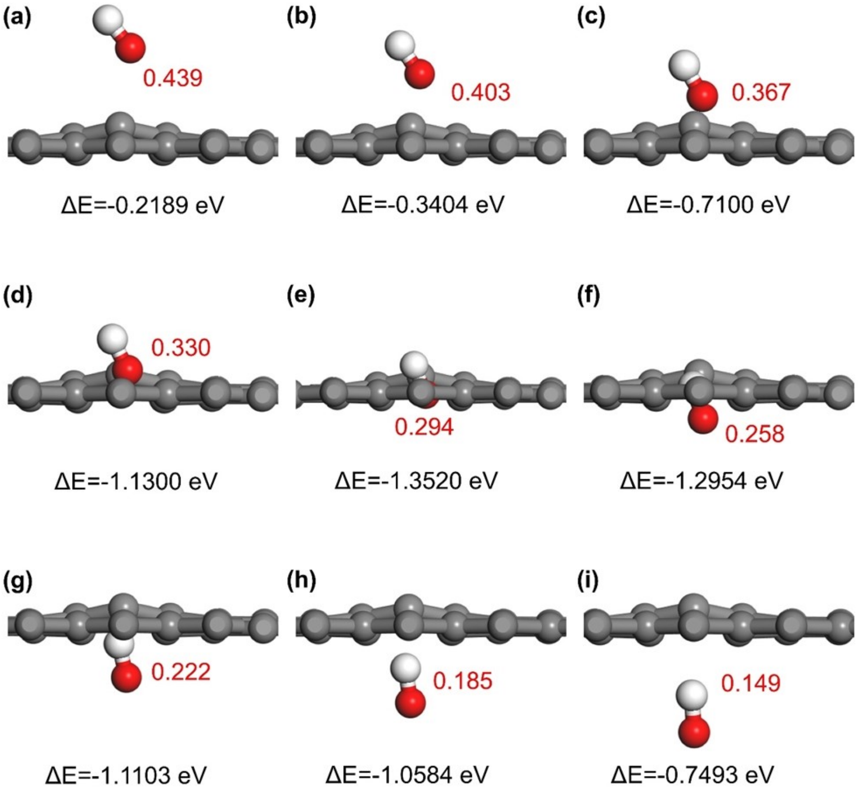

Fig. S12. Molecular structure and energy changes in each state during hydroxide ion migration.

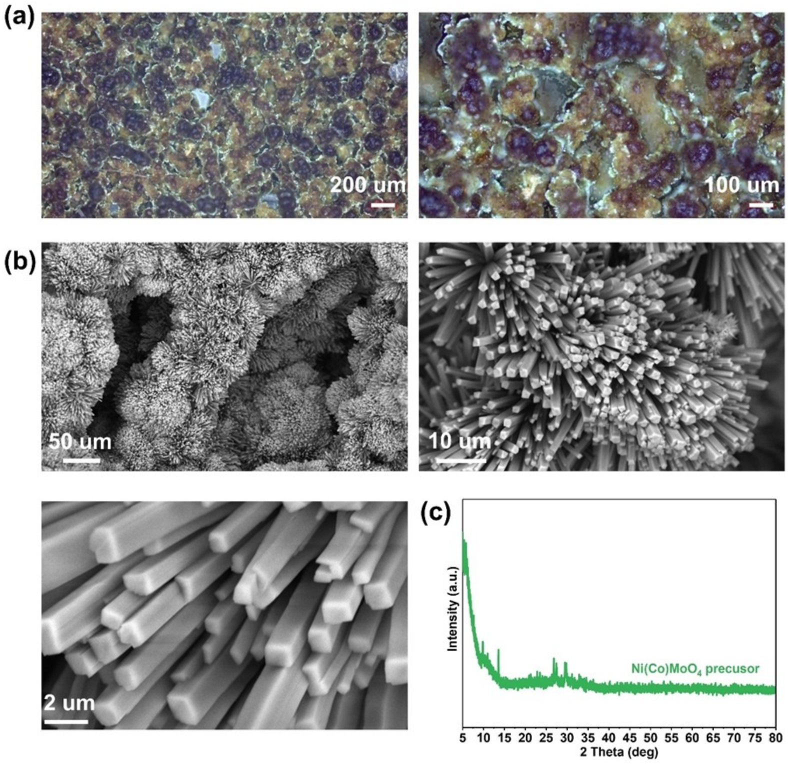

Fig. S13. (a) Metallurgical microscopy images, (b) SEM images and (c) XRD pattern of precursor Ni(Co)MoO$_4$.

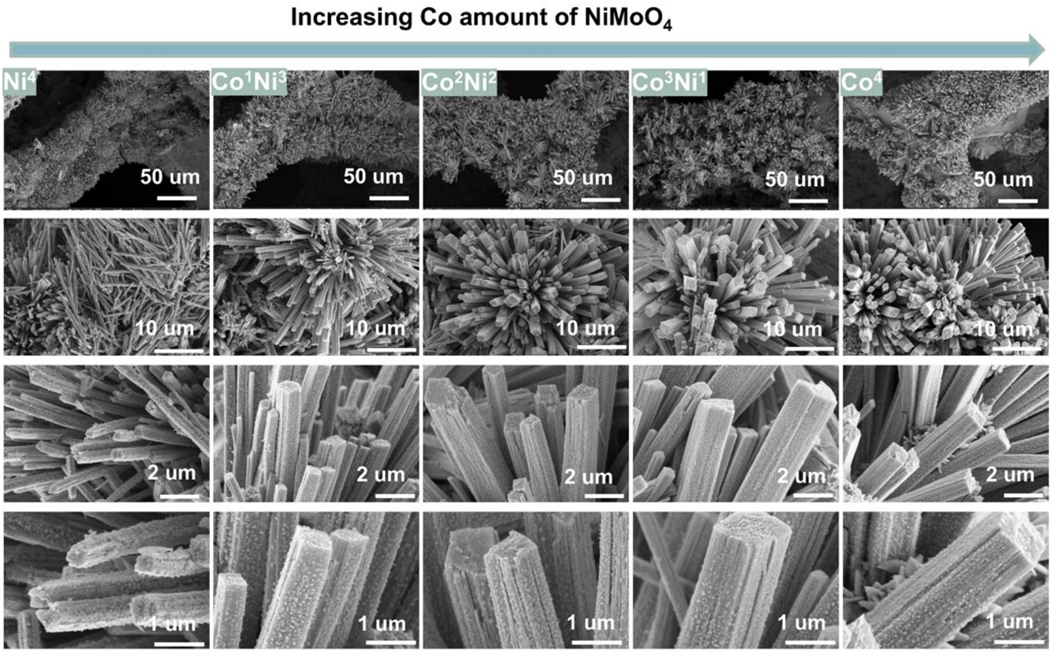

Fig. S14. SEM images of different cobalt amount of Ni(Co)MoO$_4$/MoO$_2$.

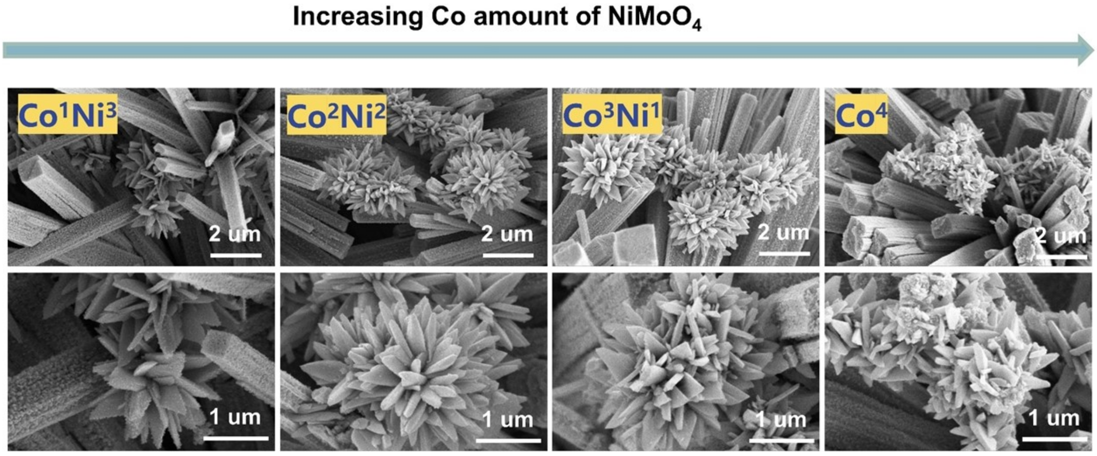

Fig. S15. SEM images of different cobalt amount of Ni(Co)MoO$_4$/MoO$_2$ accompanied by the appearance of flower-like structures.

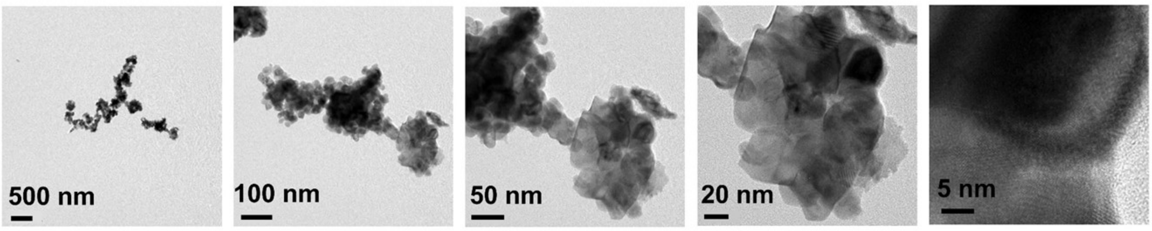

Fig. S16. TEM images of Ni(Co)MoO$_4$/MoO$_2$ accompanied by the appearance of flower-like structures.

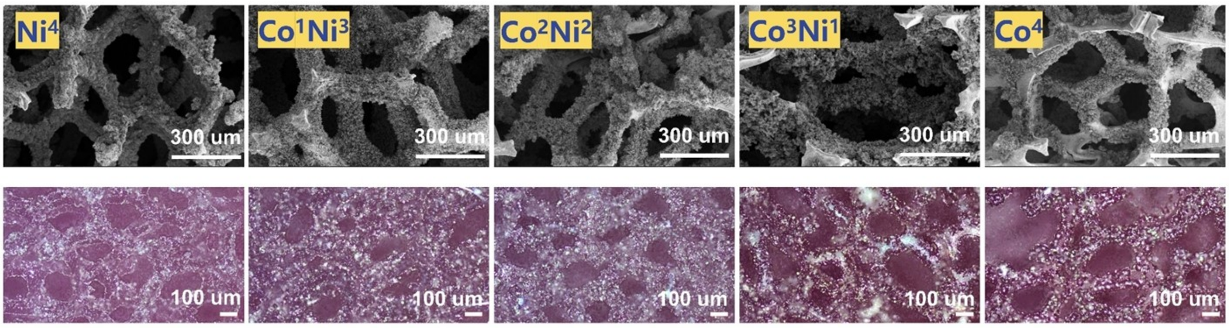

Fig. S17. Low magnification SEM images of different cobalt amount of Ni(Co)MoO$_4$/MoO$_2$.

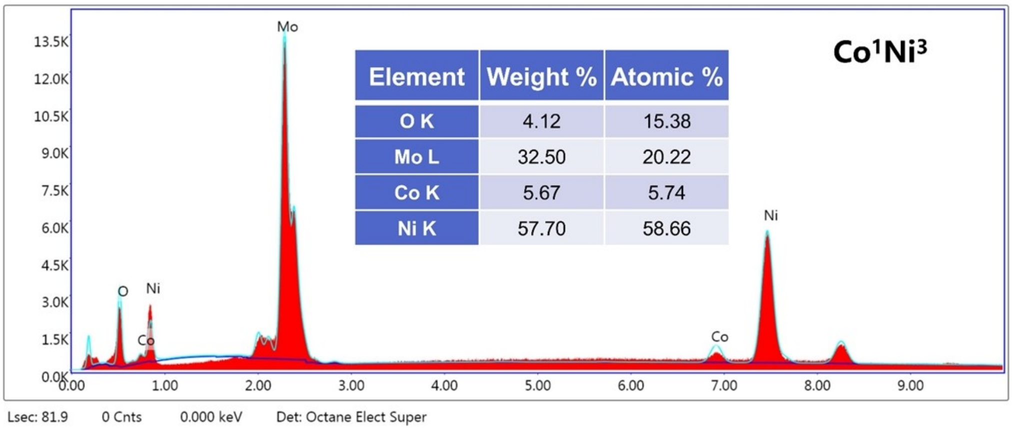

Element	Weight %	Atomic %
O K	4.12	15.38
Mo L	32.50	20.22
Co K	5.67	5.74
Ni K	57.70	58.66

Fig. S18. Energy dispersive spectroscopy analysis result of Co^{1}Ni^3 electrode.

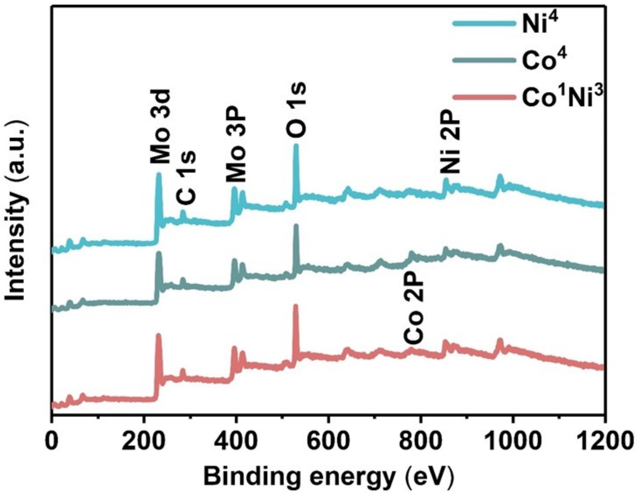

Fig. S19. XPS full spectrum of Ni^4, Co^{1}Ni^3 and Co^4 electrodes.

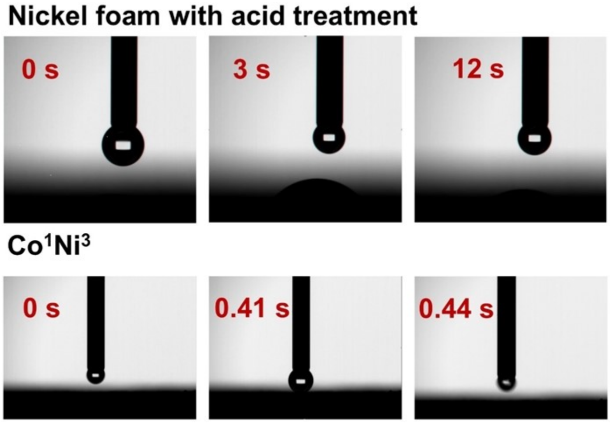

Fig. S20. Water contact angle of nickel foam and Co^1Ni^3.

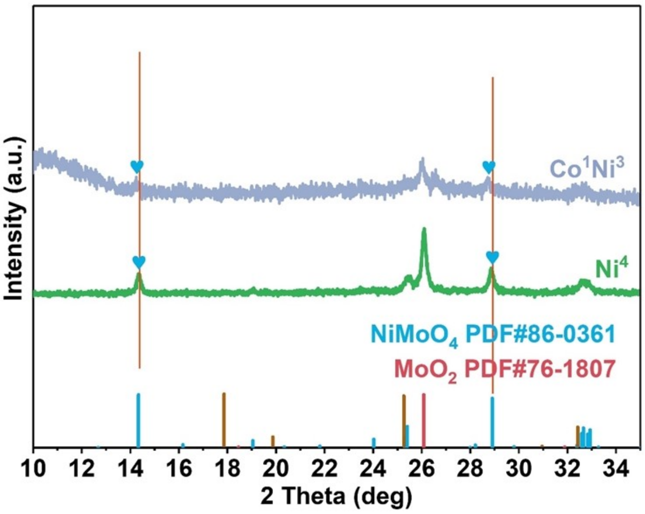

Fig. S21. XRD patterns of Ni^4 and Co^1Ni^3 electrodes.

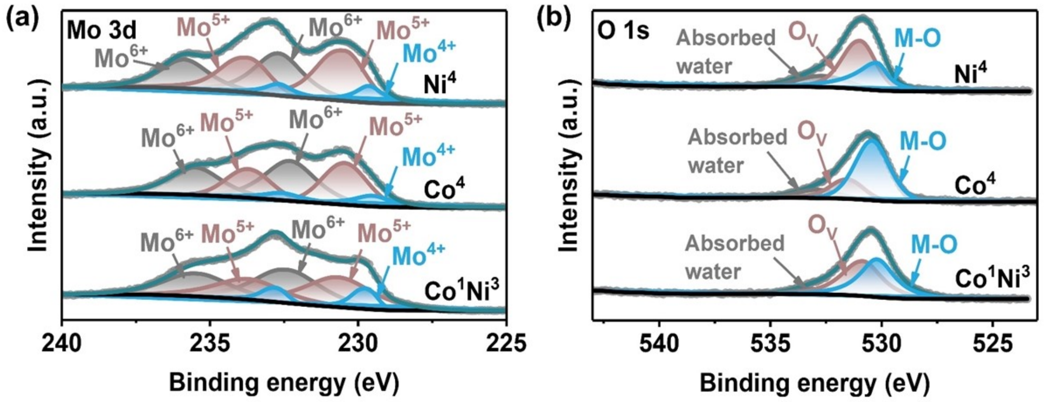

Fig. S22. XPS spectra of Mo 3d and O 1s for Co^1Ni^3, Co^4 and Ni^4 electrodes.

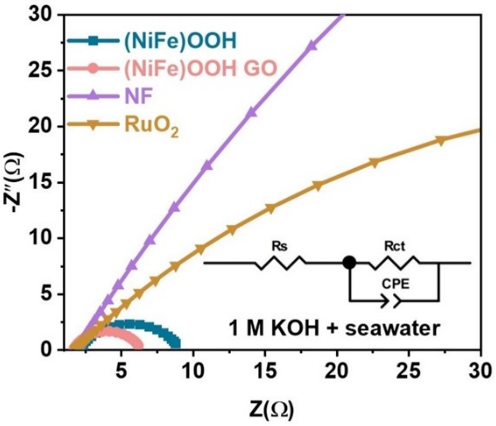

Fig. S23. The electrochemical impedance spectroscopy (EIS) results of different OER electrodes in 1.0 M KOH with seawater electrolyte.

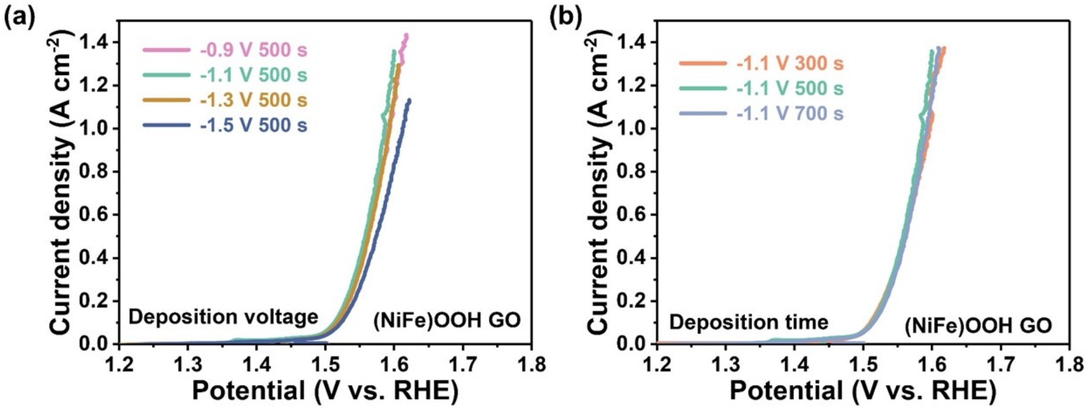

Fig. S24. OER LSV curves of (NiFe)OOH GO for different graphene oxide deposition time and voltage.

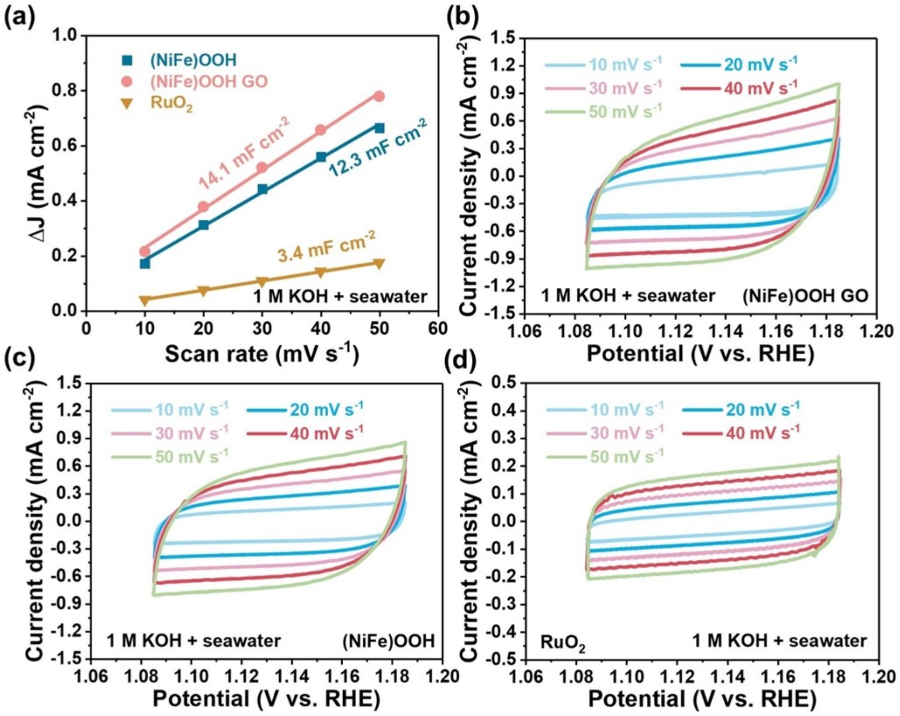

Fig. S25. Electrochemical surface area (ECSA) results of different OER electrodes in 1.0 M KOH with seawater electrolyte.

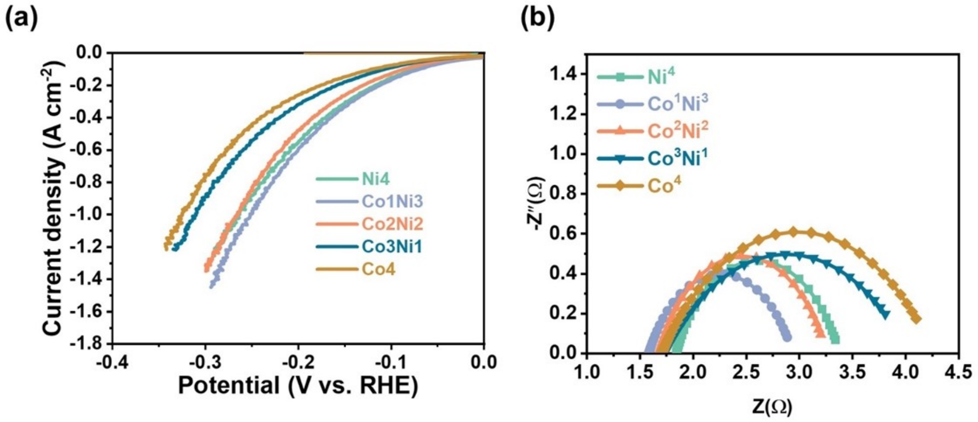

Fig. S26. HER LSV curves and EIS of different cobalt amount of Ni(Co)MoO_4/MoO_2 electrodes.

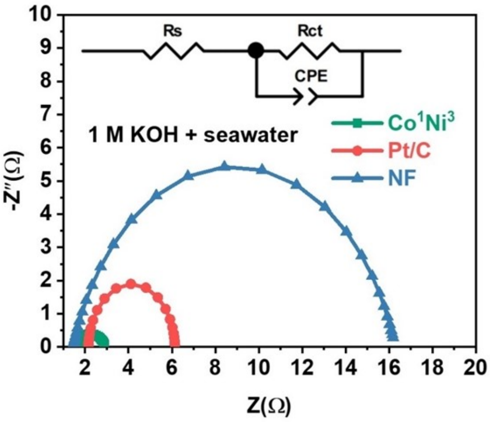

Fig. S27. EIS of different HER electrodes in 1.0 M KOH with seawater electrolyte.

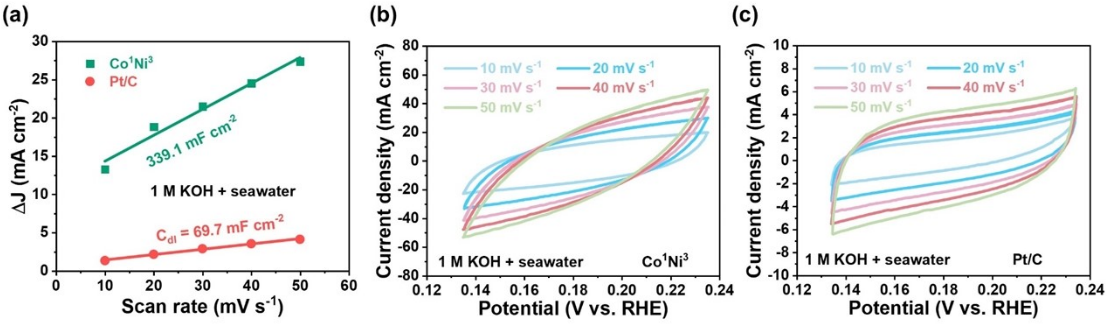

Fig. S28. Electrochemical surface area (ECSA) results of different HER electrodes in 1.0 M KOH with seawater electrolyte.

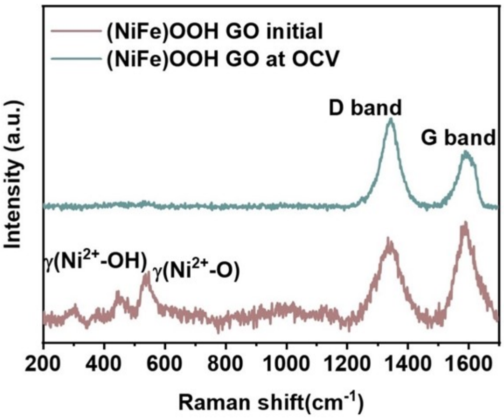

Fig. S29. Raman data for (NiFe)OOH GO electrode, and (NiFe)OOH GO electrode at open circuit voltage in 1 M KOH with seawater.

The Raman spectroscopic analysis of the (NiFe)OOH GO electrode exhibits characteristic D ($1350\,\mathrm{cm^{-1}}$) and G ($1599\,\mathrm{cm^{-1}}$) bands, with an I_D/I_G ratio of 0.87. This spectral signature confirms the presence of lattice distortions resulting from oxidative functionalization, consistent with previous reports on graphene oxide synthesis[9]. Under open-circuit potential (OCP) conditions in 1 M KOH with seawater electrolyte, the (NiFe)OOH GO electrode demonstrates a significant increase in the I_D/I_G ratio to 1.63. This enhancement reflects a substantial reduction in oxygen-containing functional groups under strongly alkaline conditions[10]. The elevated ratio corresponds to an increased defect density within the carbon lattice, indicative of partial restoration of graphitic character. From Fig. 6c, following the OER process, the I_D/I_G ratio stabilizes around 1.1, which can be attributed to the fact that the reduced graphene oxide is oxidized again during the electrooxidation process. The defect density (nD, $\mathrm{cm^{-2}}$) can be calculated using the following equations[11]:

$$nD = \frac{2.4\times10^{22} I_D}{\lambda_L^4 I_G} \tag{1.8}$$

Where λ_L is the wavelength of the laser source. Accordingly, the calculated defect density (nD) of (NiFe)OOH GO electrode, (NiFe)OOH GO electrode at OCV and (NiFe)OOH GO electrode at OER potential are $2.61\times 10^{11}\ \mathrm{cm^{-2}}$, $.4.88 \times 10^{11}\ \mathrm{cm^{-2}}$, and $3.30 \times 10^{11}\ \mathrm{cm^{-2}}$, respectively.

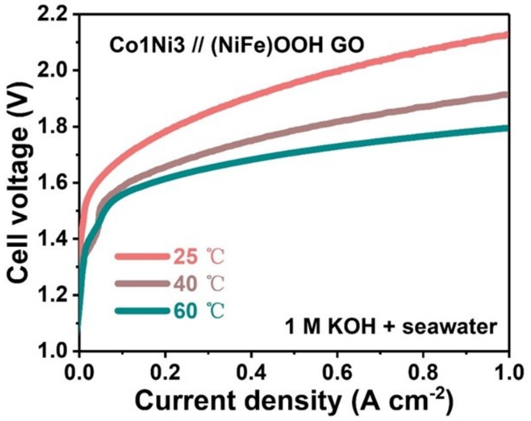

Fig. S30. Polarization curves of Co^{1}Ni^3 || (NiFe)OOH GO in 1.0 M KOH with seawater at different temperatures.

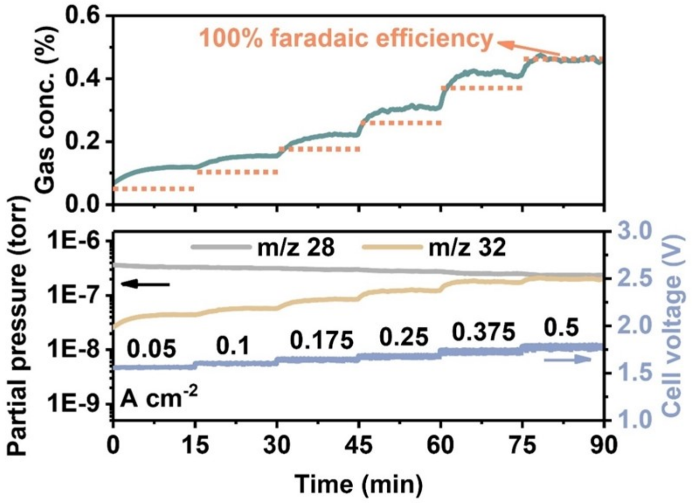

Fig. S31. FE$_{O2}$ test of Co^{1}Ni^3 || (NiFe)OOH GO in 1.0 M KOH with seawater.

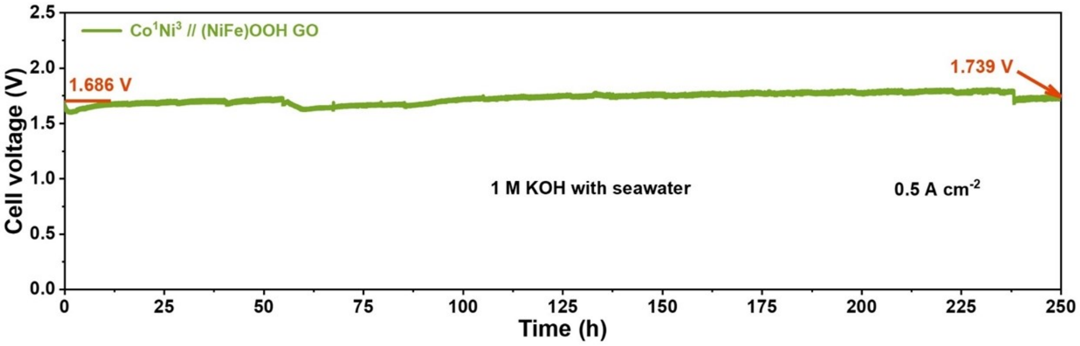

Fig. S32. Chronopotentiometry stability tests of Co^{1}Ni^3 || (NiFe)OOH GO at 500 mA cm^{-2} for seawater electrolysis.

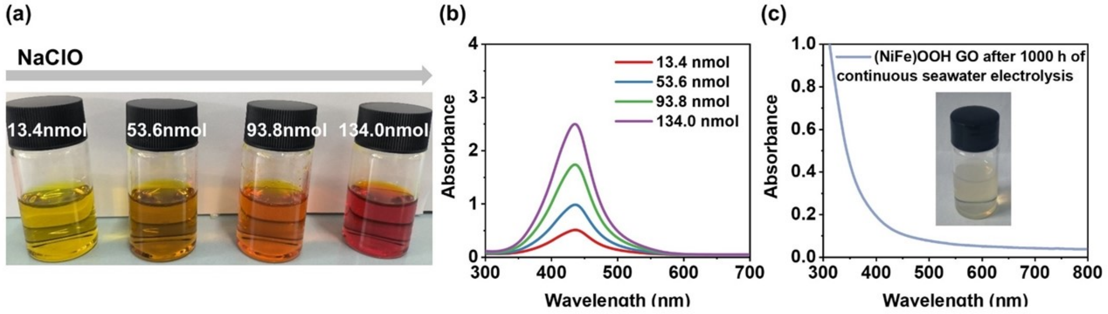

Fig. S33. (a) Photographs of the testing standard solutions between o-tolidine and different concentration of NaOCl. (b) UV-vis spectra of the testing solution following the introduction of incremental NaClO concentrations. (c) UV-vis spectra of the testing solutions after the addition of electrolyte sampled from systems after 1000 hours of continuous seawater electrolysis at 250 mA cm^{-2} current density.

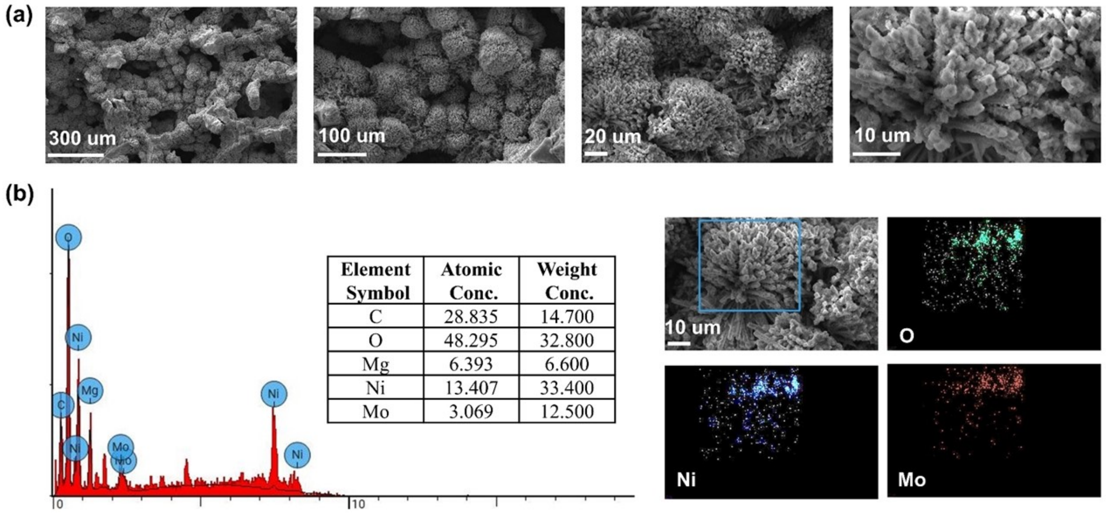

Element Symbol	Atomic Conc.	Weight Conc.
C	28.835	14.700
O	48.295	32.800
Mg	6.393	6.600
Ni	13.407	33.400
Mo	3.069	12.500

Fig. S34. Morphological structure characterization of Ni(Co)MoO_4/MoO_2 electrode after 1000 hours of continuous seawater electrolysis at 250 mA cm^{-2} current density.

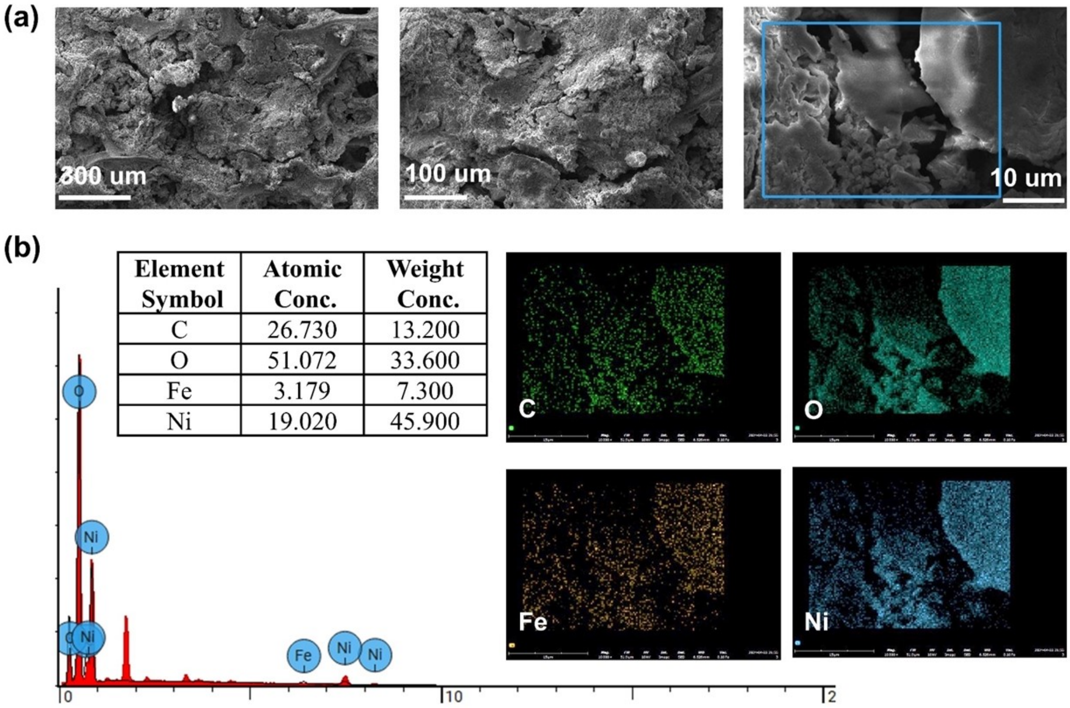

Element Symbol	Atomic Conc.	Weight Conc.
C	26.730	13.200
O	51.072	33.600
Fe	3.179	7.300
Ni	19.020	45.900

Fig. S35. Morphological structure characterization of (NiFe)OOH GO electrode after 1000 hours of continuous seawater electrolysis at 250 mA cm^{-2} current density.

Table 1. The comparison of the performances of different single electrolyzers using non-PGM-based catalysts in alkaline seawater. The electrolyte, membrane and operating temperatures of the electrolyzer are included.

AEMWEs	Electrolyte	Temperature (°C)	Membrane	Cell voltage at certain current density (V @mA cm^{-2})	References
$Ni(Co)MoO_4/MoO_2$ || $(NiFe)OOH$ GO	1.0 M KOH + seawater	60	X37-50 Grade T	1.79 V@1000 mA cm^{-2}	This work
Pt/C || Ni-doped FeOOH	1.0 M KOH + seawater	50	X37-50 Grade T	1.7 V@729 mA cm^{-2}	J. Mater. Chem. A, 2021, 9, 9586–9592
Pt/C || NiFeCo-LDH	1.0 M KOH + seawater	50	X37-50 Grade T	1.7 V@840 mA cm^{-2}	J. Energy Chem., 2022, 75, 127-134
RuMoNi || RuMoNi	1.0 M KOH + seawater	80	X37-50 Grade T	1.72 V@1000 mA cm^{-2}	Nat. Commun., 2023, 14, 3607
NiFe LDHs@NiCoS NAs/NF || (Ni,Fe)O(OH)@NiCoS NAs/NF	1.0 M KOH + seawater	60	PPT membrane	1.95 V@600 mA cm^{-2}	J. Energy Chem., 2024, 91, 370-382
Pt/C || NiFe LDH	1.0 M KOH + 0.5 M NaCl	Room temperature	Tokuyama A201	1.6 V@250 mA cm^{-2}	Adv. Energy Mater. 2018, 8, 1800338
CoP/C || NiFe LDH	1.0 M KOH + seawater	60	$PTPIm^+$ membrane	2.0 V@1000 mA cm^{-2}	ACS Energy Lett. 2023, 8, 2387−2394
$Pt/CNT(N_2H_5)_4Mo_2S_6$|| $Pt/CNT(N_2H_5)_4Mo_2S_6$	1.0 M KOH + seawater	60	X37-50 Grade T	2.0 V@1000 mA cm^{-2}	Appl. Catal. B: Environ., 2023, 338, 122996
$Co_2Mo_3O_8/MoO_2/NF$ || $Co_2Mo_3O_8/MoO_2/NF$	1.0 M KOH + seawater	50	Anion exchange membrane	2.53 V@200 mA cm^{-2} (without iR compensation)	Appl. Catal. B: Environ., 2023, 338, 123015
$Ru\text{-}Co_3O_4$ || $Ru\text{-}Co_3O_4$	1 M KOH+0.5 M NaCl+0.1 M Na_2SO_4	70	FAA-3–50	1.71 V@400 mA cm^{-2}	Appl. Catal. B: Environ., 2024, 343, 123578
$CoFe\text{-}Ni_2P$/Ni-felt || $CoFe\text{-}Ni_2P$/Ni-felt	6.0 M KOH + seawater	Room temperature	FAA-3-PK-130	2.25 V@1000 mA cm^{-2}	Adv. Energy Mater. 2023, 13, 2301475
$Fe,P\text{-}NiSe_2$ NFs || $Fe,P\text{-}NiSe_2$ NFs	0.5 M KOH + seawater	50	FAB-PK-130	1.7 V@815 mA cm^{-2}	Adv. Mater. 2021, 33, 2101425
Pt/C/NF || $(NiFe)C_2O_4/NF$	20 wt% KOH + seawater	60	Proton exchange membrane	2.4 V@500 mA cm^{-2}	Angew. Chem. Int. Ed. 2024, 63, e202316522
$MoO_x/Co(OH)_2/NF$ ||	1.0 M KOH +	Room	FAA-3–50	2.25 V@500	Nano Energy, 2024,

NiFe-LDH/NF	seawater	temperature		mA cm^{-2}	121, 109246
Fe–MoO_2/NF || Fe–MoO_2/NF	Alkaline seawater (pH = 13.8)	Room temperature	FAA-3–50	2.3 V@100 mA cm^{-2}	Mater. Horiz., 2024, 11, 1199–1211
Cu_2S@Ni || NiFeP@Ag	1 M NaOH + seawater	60	Microporous membrane	1.88 V@400 mA cm^{-2}	Adv. Mater. 2024, 36, 2306062
Pt_{SA}-$Ni_{6.6}Fe_{0.4}P_3$ || $Ni_5Fe_2P_3$	4 M NaCl + 4 M NaOH	80	Nafion 211 membrane	1.66 V@400 mA cm^{-2}	Nat. Commun., 2023, 14, 3934
PtNi mesh || Mo-Ni_3S_2/NF	Seawater and self-dampening electrolyte	Room temperature	PTFE membrane	2.3 V@400 mA cm^{-2}	Nature, 2022, 612, 673–678
Pt/h-BN || Pt/h-BN	1 M KOH + seawater	Room temperature	X37-50	3.34 V@1000 mA cm^{-2}	EcoEnergy, 2023, 1, 405–413
$Co_2P/CoMoP_2$ || $Co_2P/CoMoP_2$	1 M KOH + seawater	Room temperature	FAA-3-50	2.47 V@1000 mA cm^{-2}	Inorg. Chem. Front., 2024, 10.1039/D4QI00098F
Ru LC $Ni(OH)_2$ || jFeNi LDH	1 M KOH + seawater	80	Anion exchange membrane	1.77 V@1000 mA cm^{-2}	Angew. Chem. 2024, 136, e202317220

Reference

1 G. Kresse and J. Furthmuller, *Phys. Rev. B*, 1996, **54**, 11169−11186.

2 J. P. Perdew, K. Burke and M. Ernzerhof, *Phys. Rev. Lett.*, 1996, **77**, 3865–3868.

3 P. E. Blochl, *Phys. Rev. B*, 1994, **50**, 17953−17979.

4 G. Henkelman, B. P. Uberuaga and H. Jónsson, *J. Chem. Phys.*, 2000, **113**, 9901–9904.

5 H. Otsuka, K. Urita, N. Honma, T. Kimuro, Y. Amako, R. Kukobat, T. J. Bandosz, J. Ukai, I. Moriguchi and K. Kaneko, *Nat. Commun.*, 2024, **15**, 1708.

6 P. M. Nia, E. Abouzari-Lotf, P. M. Woi, Y. Alias, T. M. Ting, A. Ahmad and N. W. Che Jusoh, *Electrochim. Acta*, 2019, **297**, 31–39.

7 B. Qi, X. He, G. Zeng, Y. Pan, G. Li, G. Liu, Y. Zhang, W. Chen and Y. Sun, *Nat. Commun.*, 2017, **8**, 825.

8 P. Moozarm Nia, W. P. Meng, F. Lorestani, M. R. Mahmoudian and Y. Alias, *Sensor. Actuat. B: Chem.*, 2015, **209**, 100–108.

9 L. Peng, Z. Xu, Z. Liu, Y. Wei, H. Sun, Z. Li, X. Zhao and C. Gao, *Nat. Commun.*, 2015, **6**, 5716.

10 J. Zhu, X. Xiao, K. Zheng, F. Li, G. Ma, H.-C. Yao, X. Wang and Y. Chen, *Carbon*, 2019, **153**, 6–11.

11 A. Kaushal, S. K. Dhawan and V. Singh, AIP Conf. Proc., 2019, vol. 2115, p. 030106.